Lecture Notes on Magic Angle TBG

Patrick Ledwith, Eslam Khalaf, Ashvin Vishwanath

Harvard University, Cambridge MA, USA.

January 11, 2021

In these lecture notes we will attempt to give a fully analytic discussion of the essential physics of magic angle graphene. While this will necessarily involve some approximations, we hope the advantage of insight provided by these simplified models will outweigh the necessarily simplified picture they will paint. Where appropriate, we will comment on more detailed calculations and how they corroborate or modify the simple picture. :

0 Outline

1. **PART 1** Introduce a model for the band structure of magic angle graphene which can be analytically solved. Highlight the similarities with Landau level wavefunctions.
2. **PART 2** Introduce interactions and the soluble limit where U(4)x U(4) symmetry emerges and ground state can be found. Discuss simplification to spinless case U(2)xU(2) case and anisotropy calculations. Discuss derivation of the sigma models and calculation of topological term.

$$\mathcal{L}[\hat{n}_+, \hat{n}_-] = \sum_{i=\pm} \mathcal{A}[\hat{n}_i] \cdot \frac{d\hat{n}_i}{dt} - \frac{\rho}{2}|\nabla \hat{n}_i|^2 \\ -J\hat{n}_+ \cdot \hat{n}_- + (J+\lambda) n_+^z n_-^z$$

3. **PART 3** Discuss charged skyrmions, their energy versus the particle-hole excitation energy. Show that in the disordered phase of the sigma model superconductivity emerges.

1 Single Particle Electronic Structure

To set notation, let us begin with the electronic structure of graphene - by solving a tight binding model on the honeycomb lattice as show. The electron dispersion at charge neutrality (the charge

neutrality point, where one electron per atom is present, however due to spin this corresponds to filling half the states in the Brillouin Zone). The dispersion can be approximated by a Dirac equation with the following dispersion.

$$H = v_F \left(p_x \, \sigma_x \otimes \tau^0 + p_y \, \sigma_y \otimes \tau^z \right) \tag{1}$$

where $\sigma_z. = \pm 1$ corresponds to the A, B sublattices of graphene and $\tau_z = \pm 1$ corresponds to the K, K' valleys of graphene.

1.1 Single Particle Band Structure

Consider a single valley. We can write the Hamiltonian in the two layers as:

$$H_+ = \begin{bmatrix} H_{UU} & H_{UD} \\ H_{DU} & H_{DD} \end{bmatrix} \tag{2}$$

We begin with independent layers and then couple them together. The Up and Down layer Dirac Hamiltonians are:

$$\begin{aligned} H_{UU} &= v_F(-i\nabla - \mathbf{K^U}) \cdot \sigma_{\theta/2} \\ H_{DD} &= v_F(-i\nabla - \mathbf{K^D}) \cdot \sigma_{-\theta/2} \end{aligned} \tag{3}$$

where we have taken into account the shift of the Dirac points and the Pauli matrices due to rotation so that $\sigma_{\theta/2} = e^{-i\frac{\theta}{4}\sigma_z}(\sigma_x, \, \sigma_y)e^{+i\frac{\theta}{4}\sigma_z}$. We now couple the Dirac points together by interlayer hopping terms $H_{DU} = H_{UD}^\dagger$ where :

$$H_{UD} = T_0(r)\sigma^0 + T_{AB}(r)\sigma^+ + T_{BA}(r)\sigma^- \tag{4}$$

Let us now derive the form of the tunneling matrix elements - for better intuition first consider very local tunneling (i.e. electrons tunnel only when the atoms of the two layers occlude each other). We then need to consider three cases, where (i) the atoms of both sublattices are on top of each other, the so called AA or equivalently the BB regions, which form a triangular lattice see Figure 1 (ii) where the A atoms of the lower layer align with the B atoms of the upper layer (AB regions). The form one sublattice of a honeycomb lattice on the moire scale. and finally (iii) the BA regions, where B atoms of the lower layer align with the A atoms of the upper layer and form the other sublattice of the honeycomb lattice on the moire scale.

Now, tunneling say in the AA regions could be represented as: $T_0 \sim \sum_n \delta(\mathbf{r} - \mathbf{R_n})$ where the sum runs over the triangular moire lattice sites locations. From the Poisson resummation formula this can be equivalently written as $\sum_n \delta(\mathbf{r} - \mathbf{R_n}) = \frac{\mathbf{1}}{\mathbf{A_M}} \sum_{\mathbf{m}} \mathbf{e^{-iG_m \cdot r}}$, where A_M is the area of the moire unit cell and $\mathbf{G_m}$ are the moire lattice reciprocal vectors. On the other hand the tunneling matrix elements in the other regions acquire additional phase factors due to their displacement from the unit cell centers. They are $t_{AB} \sim \sum_n \delta(\mathbf{r} - \mathbf{R_n} - \mathbf{r}_A) = \frac{1}{A_M} \sum_m e^{i\mathbf{G_m \cdot r}_A} e^{-i\mathbf{G_m \cdot r}}$ and

$t_{BA} \sim \sum_n \delta(\mathbf{r} - \mathbf{R_n} - \mathbf{r}_B) = \frac{1}{A_M}\sum_m e^{i\mathbf{G_m}\cdot\mathbf{r}_B} e^{-i\mathbf{G_m}\cdot\mathbf{r}}$. In reality, one has to take into account a more general interlayer hopping $t(r)$ with Fourier components $\tilde{t}(\mathbf{G_m})$. Since the interlayer hopping depends on the 3D separation between atoms, and the separation between layers is more than twice the intra-layer atomic separations, we expect the Fourier components to decrease rapidly and we can keep the lowest order harmonics [1]. Here we will appeal to rotation symmetry. Note the original choice of $K^{U/D}$ for the Dirac points already breaks rotation symmetry. To make it more apparent we will move the Dirac points in both layers to the origin using the unitary transformation with diagonal entries: $W = e^{i\mathbf{K^U}\cdot\mathbf{r}}$, $e^{i\mathbf{K^D}\cdot\mathbf{r}}$. This leads to the following transformed Hamiltonian:

$$\begin{aligned} H'_{UU} &= v_F(-i\nabla)\cdot\sigma_{\theta/2} \\ H'_{DD} &= v_F(-i\nabla)\cdot\sigma_{-\theta/2} \end{aligned} \tag{5}$$

and denoting $\boldsymbol{q}_1 = \boldsymbol{K}^U - \boldsymbol{K}^D = k_\theta(0,-1)$, and the vectors related by $2\pi/3$ rotations $\mathbf{q_2}$, $\mathbf{q_3}$. Note the latter two differ by moire reciprocal lattice vectors and are included in the sum above.

$$H'_{UD} = w_0 U_0(r)\sigma^0 + w_1 U_{AB}(r)\sigma^+ + w_1 U_{BA}(r)\sigma^- \tag{6}$$

$$\begin{aligned} U_0(r) &= e^{-i\mathbf{q_1}\cdot\mathbf{r}} + e^{-i\mathbf{q_2}\cdot\mathbf{r}} + e^{-i\mathbf{q_3}\cdot\mathbf{r}} \\ U_{AB}(r) &= e^{-i\mathbf{q_1}\cdot\mathbf{r}} + e^{i\frac{2\pi}{3}} e^{-i\mathbf{q_2}\cdot\mathbf{r}} + e^{i\frac{4\pi}{3}} e^{-i\mathbf{q_3}\cdot\mathbf{r}} \\ U_{BA}(r) &= e^{-i\mathbf{q_1}\cdot\mathbf{r}} + e^{-i\frac{2\pi}{3}} e^{-i\mathbf{q_2}\cdot\mathbf{r}} + e^{-i\frac{4\pi}{3}} e^{-i\mathbf{q_3}\cdot\mathbf{r}} \end{aligned} \tag{7}$$

The BM Hamiltonian has the translation symmetry

$$H(\boldsymbol{r} + \boldsymbol{a}_{1,2}) = V H(\boldsymbol{r}) V^\dagger \qquad V = \mathrm{diag}(1, e^{-i\phi}, 1, e^{-i\phi}), \tag{8}$$

where the moiré lattice vectors $\boldsymbol{a}_{1,2}$ and reciprocal lattice vectors $\boldsymbol{b}_{1,2}$ are

$$\boldsymbol{a}_{1,2} = \frac{4\pi}{3k_\theta}\left(\pm\frac{\sqrt{3}}{2}, \frac{1}{2}\right), \qquad \boldsymbol{b}_{1,2} = \boldsymbol{q}_{2,3} - \boldsymbol{q}_1 = k_\theta\left(\pm\frac{\sqrt{3}}{2}, \frac{3}{2}\right). \tag{9}$$

We will find it useful to sometimes use triangular lattice and reciprocal lattice coordinates

$$r_i = \frac{\boldsymbol{r}\cdot b_i}{2\pi} \qquad k_i = \frac{\boldsymbol{k}\cdot\boldsymbol{a}}{2\pi} \tag{10}$$

which satisfy $\boldsymbol{r} = r_1\boldsymbol{a}_1 + r_2\boldsymbol{a}_2$ and $\boldsymbol{k} = k_1\boldsymbol{b}_1 + k_2\boldsymbol{b}_2$.

The relative phase shift between the top and bottom layers under translations in (8) can be understood from the misalignment of their graphene Brillouin zones due to the twist angle θ. In particular, momenta in the bottom layer are shifted by $\boldsymbol{q}_1$ relative to the top layer which generates the phase shift $e^{i\boldsymbol{q}_1\cdot\boldsymbol{a}_{1,2}} = e^{-i\phi}$ under translations. This is encoded in the form of the Bloch states

$$\psi_{\boldsymbol{k}}(\boldsymbol{r}) = u_{\boldsymbol{k}}(\boldsymbol{r}) \begin{pmatrix} e^{i(\boldsymbol{k}-\boldsymbol{K})\cdot\boldsymbol{r}} \\ e^{i(\boldsymbol{k}-\boldsymbol{K}')\cdot\boldsymbol{r}} \end{pmatrix}, \tag{11}$$

where $\boldsymbol{K}' = \boldsymbol{K} - \boldsymbol{q}_1$ is the moiré K' point wavevector in terms of the moiré K point wavevector. For zero tunneling, or large angles, the states at K (K') correspond to the top layer and bottom graphene layer respectively.

Note, in the simplest approximation $w_0 = w_1 \sim 110meV$. However, later work [8, 3] showed that inter layer relaxation, relaxation followed by intra-layer relaxation reduce the ratio $\kappa = w_0/w_1$ from unity to $\kappa = 0.8$ and further $\kappa = 0.75$. This quantity will play an important role and we will often treat it as a free parameter.

It will be particularly interesting to consider the **chiral limit**, where $\kappa = 0$. As we show in the next section, In this limit, there exists an exactly flat zero energy flat band [11].

2 A simple limiting case: The Chiral Model

We begin with the Bistritzer-Macdonald (BM) model discussed above

$$H = \begin{pmatrix} -iv\boldsymbol{\sigma}_{\theta/2} \cdot \boldsymbol{\nabla} & T(\boldsymbol{r}) \\ T^\dagger(\boldsymbol{r}) & -iv\boldsymbol{\sigma}_{-\theta/2} \cdot \boldsymbol{\nabla} \end{pmatrix} \tag{12}$$

with

$$\begin{aligned} T(\boldsymbol{r}) &= \begin{pmatrix} w_0 U_0(\boldsymbol{r}) & w_1 U_1(\boldsymbol{r}) \\ w_1 U_1^*(-\boldsymbol{r}) & w_0 U_0(\boldsymbol{r}) \end{pmatrix}, \\ U_0(\boldsymbol{r}) &= e^{-i\boldsymbol{q}_1\cdot\boldsymbol{r}} + e^{-i\boldsymbol{q}_2\cdot\boldsymbol{r}} + e^{-i\boldsymbol{q}_3\cdot\boldsymbol{r}}, \\ U_1(\boldsymbol{r}) &= e^{-i\boldsymbol{q}_1\cdot\boldsymbol{r}} + e^{i\phi}e^{-i\boldsymbol{q}_2\cdot\boldsymbol{r}} + e^{-i\phi}e^{-i\boldsymbol{q}_3\cdot\boldsymbol{r}}, \end{aligned} \tag{13}$$

The vectors $\boldsymbol{q}_i$ are $\boldsymbol{q}_1 = k_\theta(0, -1)$ and $\boldsymbol{q}_{2,3} = k_\theta(\pm\sqrt{3}/2, 1/2)$ and $\phi = 2\pi/3$.

For the following discussion we choose units where $v = k_\theta = 1$. We will also find it useful to choose the origin of the moiré BZ to be the K point to simplify some later expressions, even though the most symmetric choice is the Γ point.

A very useful appproximation to the above Hamiltonian is to set $\kappa = 0$, such that tunnelling only occurs in AB regions. Realistically we expect $\kappa \approx 0.7 < 1$ due to relaxation effects. While decreasing it all the way to zero is a drastic approximation, we will find it useful to do so at first and then examine the effects of going back to a realistic value of κ later in these notes. The model with $\kappa = 0$ is known as the chiral model because it has the chiral symmetry $\sigma_z H \sigma_z = -H$. That is, given an eigenstate $|\Psi\rangle$ of H with energy E, one can generate an eigensate $\sigma_z|\Psi\rangle$, an eigenstate with energy $-E$. Further, zero energy eigenstates can be chosen to be eigenstates of σ_z, i.e. they are sublattice polarized. Below, we will show the existence of special (magic) angles where the entire band is at zero energy. As a consequence we can define a sublattice polarized basis for these eigenstates. What is less obvious is that these sublattice polarized bands also carry Chern number of one, and in fact share many similarities, in ways that will be made precise below, with the lowest Landau level.

The chiral symmmetry is especially useful at the magic angle; here we obtain *exactly* flat bands at zero energy that are eigenstates of σ_z. Since we are interested in zero modes that are eigenstates

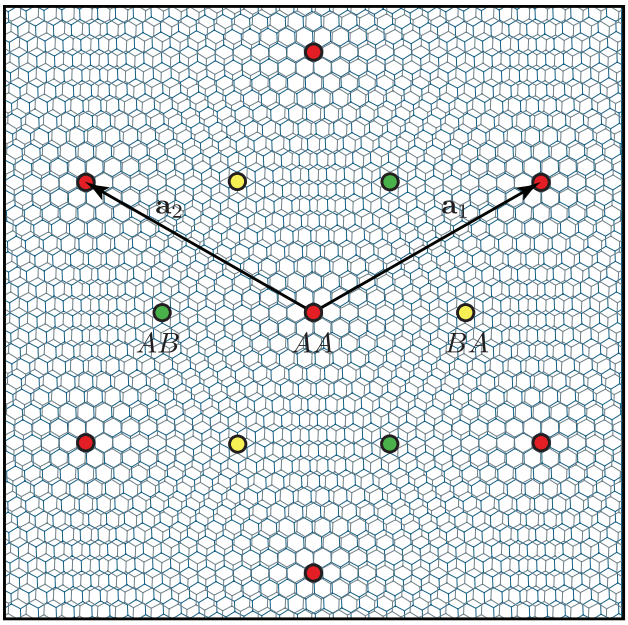

Figure 1: Real space visualization of the moiré pattern and depiction of the AA stacking $\boldsymbol{r} = 0$, AB stacking $\boldsymbol{r} = -\boldsymbol{r}_0$, and BA stacking $\boldsymbol{r} = \boldsymbol{r}_0$ points. All three of these points map to themselves up to shifts by lattice vectors under C_3 symmetry

of σ_z, we rewrite the Hamiltonian by exchanging the second and third columns after which $\sigma_z = \text{diag}(1, 1, -1, -1)$ and

$$H = \begin{pmatrix} 0 & D^\dagger \\ D & 0 \end{pmatrix} \quad D = \begin{pmatrix} -2i\overline{\partial} & \alpha U_1(\boldsymbol{r}) \\ \alpha U_1(-\boldsymbol{r}) & -2i\overline{\partial} \end{pmatrix}, \tag{14}$$

with $\alpha = w_1 = w_1/vk_\theta$. Because $\{H, \sigma_z\} = 0$, zero energy solutions may be chosen to be eigenstates of σ_z. We therefore search for solutions to the equation $D\psi_{\boldsymbol{k}}(\boldsymbol{r}) = 0$ for each moiré Bloch momentum $\boldsymbol{k}$. The solutions when $\sigma_z = -1$ can be obtained using $C_2\mathcal{T}$ symmetry: $\chi_{\boldsymbol{k}}(\boldsymbol{r}) = \psi^*_{\boldsymbol{k}}(-\boldsymbol{r})$.

Zero Modes of Chiral Model: When $\boldsymbol{k} = K$, we are guaranteed a zero mode solution by continuity from $\alpha = 0$, i.e. the unperturbed Dirac points in the two layers. This is because the zero mode $\psi_K = \begin{pmatrix} 1 & 0 \end{pmatrix}^T$ is pinned to zero energy because it is an eigenstate of σ_z and it cannot move to different values of $\boldsymbol{k}$ because it is pinned to $\boldsymbol{k} = K$ by C_3 symmetry. Thus ψ_K has zero energy for all $\alpha > 0$.

Next we note that because D only has antiholomorphic derivatives $D\left(F(z)\psi_K(\boldsymbol{r})\right) = F(z)D\psi_K(\boldsymbol{r}) = 0$ for any holomorphic function $F(z)$ where $z = x + iy$. However, any holomorphic function $F(z)$ is either constant or blows up at infinity by Liouville's theorem. Hence, this state cannot be a Bloch state at a momentum other than K. At this point it may appear that we cannot obtain zero modes except at isolated crystal momenta. However there is way out - we can allow $F(z)$ to be a meromorphic function. Although such a function would necessarily have poles at certain positions in the unit cell, we could arrange for them to be precisely cancelled by zeros in $\psi_K(\boldsymbol{r})$. Note, since this is a spinor wavefunction, we will need both components of $\psi_K(\boldsymbol{r})$ to simultaneously vanish at that location in the unit cell. We can explore if such a condition is satisfied by varying the angle. Indeed the magic angles are precisely those angles for which ψ_K has a zero in both of its components at some $\boldsymbol{r}$.

In fact, symmetry helps us locate where the zero will appear. We focus on the points $\pm\boldsymbol{r}_0$, the BA/AB stacking points respectively with $\boldsymbol{r}_0 = \frac{1}{3}(\boldsymbol{a}_1 - \boldsymbol{a}_2) = 0$. These points are distinguished by C_3 symmetry since they map to themselves up to a lattice vector, $C_3\boldsymbol{r}_0 = \boldsymbol{r}_0 + \boldsymbol{a}_2$, see Fig.1). We show that three fold rotation symmetry implies that one of the components $\psi_{K2}(\pm\boldsymbol{r}_0) = 0$. Indeed, C_3 symmetry implies $\psi_K(R_\phi\boldsymbol{r}) = \psi_K(\boldsymbol{r})$ where R_ϕ rotates vectors by an angle ϕ. One may deduce that this is the correct representation by continuity from $\alpha = 0$ where $\psi_K = (1, 0)^T$. However, we additionally have

$$\psi_{K2}(\pm\boldsymbol{r}_0) = \psi_{K2}(\pm R_\phi\boldsymbol{r}_0) = \psi_{K2}(\pm\boldsymbol{r}_0 \pm \boldsymbol{a}_2) = e^{\mp i\phi}\psi_{K2}(\boldsymbol{r}_0) \tag{15}$$

since due to the form of the Bloch states (8) the second component of ψ_K picks up a phase under translations.

While it is possible to show that $D\psi_K = 0$ does not allow for $\psi_{K1}(-\boldsymbol{r}_0) = 0$, it is possible for the single component $\psi_{K1}(\boldsymbol{r}_0) = 0$ (which can be chosen real) by tuning the angle. Thus we have one tuning parameter to set a single real number to zero, which generically will give a series of points as solutions, i.e. magic angles. The first of these angles is at nearly the same angle as realistic TBG and can be approximated using perturbation theory for small α. In particular, we plug in the ansatz

$$\psi_K = \begin{pmatrix} 1 + \alpha^2 u_2 + \cdots \\ \alpha u_1 + \cdots \end{pmatrix} \tag{16}$$

to the zero mode equation $D\psi_K = 0$ and obtain

$$u_1 = -i(e^{i\boldsymbol{q}_1\cdot\boldsymbol{r}} + e^{i\boldsymbol{q}_1\cdot\boldsymbol{r}} + e^{i\boldsymbol{q}_1\cdot\boldsymbol{r}}) \quad u_2 = \frac{i}{\sqrt{3}}e^{-i\phi}(e^{-i\boldsymbol{b}_1\cdot\boldsymbol{r}} + e^{i\boldsymbol{b}_2\cdot\boldsymbol{r}} + e^{i(\boldsymbol{b}_1-\boldsymbol{b}_2)\cdot\boldsymbol{r}}) + \text{c.c.} \tag{17}$$

We then compute $u_1(\boldsymbol{r}_0) = 0$ and $u_2(\boldsymbol{r}_0) = -3$ such that when $\alpha \approx 1/\sqrt{3} \approx 0.577$ the entire spinor vanishes. The perturbation expansion may be carried out to higher orders and seems to get arbitrarily close to the numerically obtained value of $\alpha_1 \approx 0.586$ for the first chiral magic angle. There seem to be infinitely many α for which ψ_K vanishes with the quasiperiodicity $\alpha_n \approx \alpha_{n-1} + 1.5$ holding for large α. Other metrics such as vanishing of Dirac velocity, maximum gap to neighboring bands and minimum bandwidth also gives the same result. See ref. [11] for more details.

Wavefunctions: To generate the rest of the states in the band we need to choose a meromorphic function $F_{\boldsymbol{k}}(z)$ that is Bloch periodic. To do so, we write $F_{\boldsymbol{k}}(z) = f_{\boldsymbol{k}}(z)/g(z)$ where both $f_{\boldsymbol{k}}$ and g are holomorphic and $g(z_0 + ma_1 + na_2) = 0$ where $z_0 = r_{0x} + ir_{0y}$ and similarly $a_{1,2}$ are the complex number versions of the lattice vectors $\boldsymbol{a}_{1,2}$. The only choice for $g(z)$, up to multiplication by an exponential function, is the Jacobi theta function.

$$g(z) = \vartheta_1\left(\frac{z - z_0}{a_1}\middle| e^{i\phi}\right), \qquad \vartheta(u|\tau) = -i\sum_{n=-\infty}^{\infty}(-1)^n e^{\pi i\tau\left(n+\frac{1}{2}\right)^2 + \pi i(2n+1)u} \tag{18}$$

Under translations the Jacobi theta function satisfies

$$\vartheta_1(u+1|\tau) = -\vartheta_1(u|\tau), \qquad \vartheta_1(u+\tau|\tau) = -e^{-\pi i\tau - 2\pi iu}\vartheta_1(u|\tau). \tag{19}$$

and $\vartheta_1(0|\tau) = 0$ such that $g(z)$ has the desired zeros (note that a translation by $\boldsymbol{a}_1$ shifts argument of the theta function by 1 while a translation by $\boldsymbol{a}_2$ shifts the argument of the theta function by $a_2/a_1 = e^{i\phi} = \tau$). The properties (19) enable us to construct Bloch states by choosing $f_{\boldsymbol{k}}(z)$ to also be a theta function, since although a single theta function is only an eigenstate under translations

in one direction, the above u dependence in translations proportional to τ will always cancel out in any ratio of theta functions leaving a pure phase. This pure phase may be manipulated by shifting the arguments of the theta functions relative to each other, and an exponential function can also be included as an additional knob. We may therefore engineer $f_{\boldsymbol{k}}(z) = e^{2\pi i k_1 z/a_1}\vartheta_1((z-z_0)/a_1 - k/b_2|e^{i\phi})$ for $k = k_x + ik_y$ (measured from the K point) such that

$$\begin{aligned}\psi_{\boldsymbol{k}}(\boldsymbol{r}) &= e^{2\pi i k_1 z/a_1}\vartheta_1\left(\frac{z-z_0}{a_1} - \frac{k}{b_2}\middle| e^{i\phi}\right)\frac{\psi_K(\boldsymbol{r})}{\vartheta_1\left(\frac{z-z_0}{a_1}|e^{i\phi}\right)},\\ u_{\boldsymbol{k}}(\boldsymbol{r}) &= e^{-i\boldsymbol{k}\cdot\boldsymbol{r}}\psi_{bk}(\boldsymbol{r}) = e^{-2\pi i r_2 k/b_2}\vartheta_1\left(\frac{z-z_0}{a_1} - \frac{k}{b_2}\middle| e^{i\phi}\right)\frac{u_K(\boldsymbol{r})}{\vartheta_1\left(\frac{z-z_0}{a_1}|e^{i\phi}\right)}.\end{aligned} \tag{20}$$

are Bloch periodic and periodic under translations respectively.

Let us make two observations - first, note the functional dependence of Bloch wavefunctions $u_{\boldsymbol{k}}(\boldsymbol{r})$ on moving through the BZ. In the gauge we have chosen, the entire dependence is via $k = k_x + ik_y$, i.e. it is an *analytic* function of k.Next, note that these wavefunctions describe a Chern band with $C = +1$. The $C_2\mathcal{T}$ related band with $\sigma_z = -1$ then has $C = -1$. Including the bands from the other graphene valley and spin degeneracy, we obtain four exactly flat bands with $C = +1$ and four exactly flat bands with $C = -1$.

Such a situation seems extremely close to that of quantum Hall ferromagnetism with two important differences. The first is that there is an extra time reversed copy with opposite Chern numbers. The second is that these flat bands are not precisely the same as the lowest Landau level. How can we understand and quantify the latter distinction? The coarse indicators of flat dispersion and Chern number are the same.

Quantum Geometry of the Chiral Flat Bands: To understand the similarities and differences between the flat TBG bands and Landau levels we review how to characterize the geometry of a band. We begin by considering the Bloch overlaps, or form factors, $\langle u_{\boldsymbol{k}_1}|u_{\boldsymbol{k}_2}\rangle$ that appears in any physical quantity that is indifferent to the "internal" indices of the wavefunctions: in the case of chiral TBG, this is layer and the position $\boldsymbol{r}$ within a unit cell. There are two important aspects of these overlaps: their phase and magnitude. The bare phase is not gauge invariant, but if we consider the phase of an overlap that traces a small loop in $\boldsymbol{k}$-space we obtain a gauge invariant quantity from which we may extract the Berry curvature:

$$\begin{aligned}\Omega(\boldsymbol{k}) &= \lim_{q\to 0} q^{-2}\,\mathrm{Im}\mathrm{P}(\boldsymbol{k})\\ P(\boldsymbol{k}) &= \left\langle u_{\boldsymbol{k}-\frac{q\hat{x}}{2}-\frac{q\hat{y}}{2}}\middle| u_{\boldsymbol{k}+\frac{q\hat{x}}{2}-\frac{q\hat{y}}{2}}\right\rangle\left\langle u_{\boldsymbol{k}+\frac{q\hat{x}}{2}-\frac{q\hat{y}}{2}}\middle| u_{\boldsymbol{k}+\frac{q\hat{x}}{2}+\frac{q\hat{y}}{2}}\right\rangle\left\langle u_{\boldsymbol{k}+\frac{q\hat{x}}{2}+\frac{q\hat{y}}{2}}\middle| u_{\boldsymbol{k}-\frac{q\hat{x}}{2}+\frac{q\hat{y}}{2}}\right\rangle\left\langle u_{\boldsymbol{k}-\frac{q\hat{x}}{2}+\frac{q\hat{y}}{2}}\middle| u_{\boldsymbol{k}-\frac{q\hat{x}}{2}-\frac{q\hat{y}}{2}}\right\rangle\end{aligned} \tag{21}$$

On the other hand, there is information contained in the magnitude of the Bloch overlaps as well that the Berry curvature does not take into account. This is encapsulated by a quantum distance between $\boldsymbol{k}$-points and associated Fubini-Study metric

$$D(\boldsymbol{k}_1,\boldsymbol{k}_2) = 1 - |\langle u_{\boldsymbol{k}_1}|u_{\boldsymbol{k}_2}\rangle|, \qquad g_{ab}(\boldsymbol{k}) = \frac{\partial}{\partial q_a}\frac{\partial}{\partial q_b}D(\boldsymbol{k},\boldsymbol{k}+\boldsymbol{q})\big|_{\boldsymbol{q}=0} \tag{22}$$

The Berry curvature and Fubini-Study metric are tied together in special systems. One may see this by constructing a gauge invariant complex tensor sometimes referred to as the "quantum metric"

which is schematically written as $\eta = g + 2i\epsilon\Omega$, where g is the symmetric F-S metric and ϵ is the antisymmetric matrix. This can be compactly written in terms of the gauge invariant projector $Q(k)$ as:

$$\eta_{ab}(\boldsymbol{k}) = \frac{\langle \partial_{k_a} u_{\boldsymbol{k}}| \, Q(\boldsymbol{k}) \, |\partial_{k_b} u_{\boldsymbol{k}}\rangle}{\langle u_{\boldsymbol{k}}|u_{\boldsymbol{k}}\rangle} \quad Q(\boldsymbol{k}) = 1 - \frac{|u_{\boldsymbol{k}}\rangle \, \langle u_{\boldsymbol{k}}|}{\langle u_{\boldsymbol{k}}|u_{\boldsymbol{k}}\rangle}. \tag{23}$$

The quantum metric is Hermitian and positive semidefinite because it proportional to a projection of $Q(\boldsymbol{k})$ onto the subspace spanned by the states $|\partial_{k_x} u_{\boldsymbol{k}}\rangle$ and $\left|\partial_{k_y} u_{\boldsymbol{k}}\right\rangle$, and $Q(\boldsymbol{k})$ is manifestly Hermitian and positive semidefinite as a projection operator. The real and imaginary components of η can be seen to correspond to the Fubini Study metric and Berry curvature respectively

$$\Omega = -2\mathrm{Im}\,\eta_{\mathrm{xy}} = 2\mathrm{Im}\,\eta_{\mathrm{yx}} \quad \mathrm{g_{ab}} = \mathrm{Re}\,\eta_{\mathrm{ab}} \tag{24}$$

and the fact that η is positive semidefinite, $\det \eta \geq 0$, implies that $\det g(\boldsymbol{k}) \geq |\Omega(\boldsymbol{k})|^2/4$. The inequality is saturated for all two band systems, as well as other special systems. A stronger condition that very few systems satisfy is obtained if we additionally require that the eigenvectors of $g(\boldsymbol{k})$ are the *same* for all $\boldsymbol{k}$. This is not implied by any rotation symmetry, as the rotation symmetry changes the value of $\boldsymbol{k}$. In this case, we may simultaneously diagonalize $g(\boldsymbol{k})$ at all values of $\boldsymbol{k}$ and obtain

$$g_{ij}(\boldsymbol{k}) = \frac{1}{2}|\Omega(\boldsymbol{k})|\delta_{ij} \tag{25}$$

We will soon show that (25) is satisfied exactly by the *lowest* Landau level (which further satisfies $\Omega(\boldsymbol{k})$ independent of $\boldsymbol{k}$) as well as chiral TBG. It is strongly violated for all higher Landau levels. Such a distinction is important because the physics of higher Landau levels is very different from the lowest Landau level, even though all Landau levels are flat and have identical Berry curvature and Chern number. In particular, most fractional quantum Hall states are observed in the lowest Landau level, and none are observed for the second and higher Landau levels.

Notably, if the Bloch states $|u_{\boldsymbol{k}}\rangle$ can be chosen to be holomorphic in $k = k_x + ik_y$, then (25) is satisfied. The reason can be seen directly from (23) upon replacing $\partial_{k_x} u_k = (\partial_k + \overline{\partial}_k)u_k = \partial_k u_k$ and similarly $\partial_{k_y} u_k = i\partial_k u_k$. We then obtain

$$\eta(\boldsymbol{k}) \propto \begin{pmatrix} 1 & i \\ -i & 1 \end{pmatrix} \tag{26}$$

from which (25) follows. This is the reason why the lowest Landau level Bloch states satisfy (25), and in that case continuous magnetic translation symmetry additionally implies that $\Omega(\boldsymbol{k})$ is independent of $\boldsymbol{k}$.

For chiral TBG there is no continuous magnetic translation symmetry, but the wavefunctions $u_{\boldsymbol{k}}$ in (20) are in fact holomorphic in k. We ensured this by carefully choosing $f_{\boldsymbol{k}}(z)$, but such a choice was always possible because the zero mode operator D only contains antiholomorphic derivatives. Indeed, acting on $u_{\boldsymbol{k}}$ the zero mode equation has the form

$$\begin{pmatrix} -2i\overline{\partial} - k & \alpha U(\boldsymbol{r}) \\ \alpha U(\boldsymbol{r}) & -2i\overline{\partial} - k - q_1 \end{pmatrix} u_{\boldsymbol{k}}(\boldsymbol{r}) = 0. \tag{27}$$

Because $u_{\boldsymbol{k}}$ is a zero mode of an operator that is independent of $\bar{k}$, it may also be chosen to be independent of $\bar{k}$.

In fact, the chiral TBG wavefunctions are closely related to LLL wavefunctions. Indeed we may write them in the form

$$\psi_{\boldsymbol{k}}(\boldsymbol{r}) = e^{2\pi i k_1 z/a_1}\vartheta_1\left(\frac{z-z_0}{a_1} - \frac{k}{b_2}|e^{i\phi}\right) e^{-K(\boldsymbol{r})}\begin{pmatrix} u_1(\boldsymbol{r}) \\ u_2(\boldsymbol{r})\end{pmatrix} \tag{28}$$

with

$$e^{-K(\boldsymbol{r})} = \frac{\|\psi_K(\boldsymbol{r})\|}{\left|\vartheta_1\left(\frac{z-z_0}{a_1}|e^{i\phi}\right)\right|}, \tag{29}$$

as the analogue of the Landau gauge factor $e^{-y^2/2\ell_B^2}$ and $u_i(\boldsymbol{r}) = e^{K(\boldsymbol{r})}\psi_{Ki}(\boldsymbol{r})/\vartheta_1\left(\frac{z-z_0}{a_1}|e^{i\phi}\right)$ are components of a normalized layer-spinor. This normalized layer spinor is independent of $\boldsymbol{k}$ and so drops out of all Bloch overlaps; it has no influence on band geometry. The wavefunction obtained by stripping off the layer spinor

$$\tilde{\psi}_{\boldsymbol{k}}(\boldsymbol{r}) = e^{2\pi i k_1 z/a_1}\vartheta_1\left(\frac{z-z_0}{a_1} - \frac{k}{b_2}\middle|e^{i\phi}\right) e^{-K(\boldsymbol{r})} \tag{30}$$

is the Bloch state for a Dirac particle in an inhomogeneous, moiré periodic, magnetic field $B(\boldsymbol{r}) = \frac{\hbar}{e}\nabla^2 K(\boldsymbol{r})$. See [6] for further details.

3 Interaction Effects at Integer Fillings

In this section we begin by recounting the absolute simplest example of ferromagnetism in quantum Hall systems at unit filling in the lowest Landau level. An excellent reference is Girvin's Les Houches Lecture Notes [4].

3.1 Quantum Hall Ferromagnetism:

The setup is as follows. Electrons in the lowest landau level are at filling $\nu = 1$. Naturally an integer quantum Hall state is formed. The question that remains is about the spin degeneracy. Athough Zeeman coupling splits the spin degeneracy, this is often a weak effect, particularly if the g factor is small. In fact, interactions lead to a spontaneous ferromagnet even in the absence of Zeeman field. Furthermore the expected energy gaps are set by the interaction strength, and much larger than the typical Zeeman splitting. The spontaneous ferromagnet has Goldstone modes characterized by a stiffness. Most interestingly, a consequence of the Chern number of the Landau level is that there is an entanglement between spin and charge degrees of freedom. Topological textures of spin (skyrmions) carry electric charge. Let us briefly describe this below and transcribe this to our more complex, but similar setting of magic angle TBG. The most important differences will be, first, that in addition to spin, valley quantum number will also be present. Second, given the obvious time reversal symmetry, a mirror sector with opposite magnetic field or equivalents, opposite Chern number will be present. This is shown in the table below.

There are some important consequences of the contrast from the quantum Hall case, i.e. arising from the fact that here a pair of quantum Hall ferromagnets with opposite Chern number. These are coupled together by a superexchange interaction J, which locks them into an antiferromagnetic

	Quantum Hall Ferromagnet	TBG
Ground State	Ferromagnet at $\nu = 1$	Flavor Order at $\nu =$ integer
Single particle excitations	Gapped: $\Delta =$	Gapped Insulator
Collective modes	Spin waves stiffness $\rho =$	Flavor waves
Effective Theory	$\mathcal{L}_C[\hat{n}] = \mathcal{L}_{\rm B} + \rho(\nabla\hat{n})^2 + i\frac{\epsilon^{\mu\nu\lambda}}{4\pi}CA_\mu\hat{n}\cdot\partial_\nu\hat{n}\times\partial_\lambda\hat{n}$	$\mathcal{L}_+[\hat{n}_+] + \mathcal{L}_-[\hat{n}_-] + J\hat{n}_+\cdot\hat{n}_-$

Table 1: Comparison between Quantum Hall ferromagnetism and twisted bilayer graphene (TBG). In the last row, $\mathcal{L}_{\rm B}$ is the Berry phase for spin 1/2, and the last row and column describes the effective theory for a simplified 'spinless' TBG.

configuration. We will see that corresponding to the Skyrmions of the integer quantum Hall effect, in this TBG model the skyrmions will carry twice the charge and correspond to Cooper pairs. Also, an important distinction is that there is an effective time reversal symmetry here than ensures skyrmions have an effective mass and do not see a net Lorentz force. This is in contrast to IQH skyrmions that effectively experience a strong Lorentz force from the large effective magnetic field from the ferromagnetic moments.

3.2 Projection onto the flat bands

Let us now turn our attention back to twisted bilayer graphene and discuss the effect of adding the Coulomb interaction to the flat bands. Our main assumption is that the gap to the remote bands Δ is much larger than the scale for the Coulomb interaction which is given by $V_0 = \frac{e^2}{4\pi\epsilon\epsilon_0 L_M}$ where ϵ is the relative permittivity and L_M is the Moiré length. For parameters typical to TBG, V_0 is around 10-20 meV whereas the gap Δ is close to 100 meV in the chiral limit (in the realistic model, the gap is reduced to about 40 meV). This is similar to projecting into the lowest Landau level.

To consider the interacting problem, we need to take into account the existence of two graphene valleys K and K' which in addition to spin degeneracy yields a fourfold flavor degeneracy. Combined with the two-fold degeneracy of the flat bands, this means we have 8 flat bands in total. These flat bands are labelled by a spin $s =\uparrow / \downarrow$, valley $\tau = K/K'$ and sublattice $\sigma = A/B$ indices. We will find it convenient to combine these 3 indices into an 8 component index $\alpha = (s, \tau, \sigma)$ labeling the states within the 8-dimensional space of flat bands at a given momentum. Our task is to understand the nature of the ground state at various filling ν. By convention $\nu = 0$ refers to the charge neutrality point and $\nu = \pm 4$ refers to full and empty bands. We will be particularly interested in integer fillings, where an insulator can be stabilized even without enlarging the Moiré unit cell. The following analysis follows closely Ref. [2].

The interacting Hamiltonian projected onto the flat bands have the form

$$\mathcal{H} = \sum_{\alpha,\boldsymbol{k}\in\mathrm{MBZ}} c^\dagger_{\alpha,\boldsymbol{k}} h_{\alpha,\beta}(\boldsymbol{k}) c_{\beta,\boldsymbol{k}} + \frac{1}{2A}\sum_{\boldsymbol{q}} V_{\boldsymbol{q}}\delta\rho_{\boldsymbol{q}}\delta\rho_{-\boldsymbol{q}}, \qquad \delta\rho_{\boldsymbol{q}} = \rho_{\boldsymbol{q}} - \bar{\rho}_{\boldsymbol{q}} \tag{31}$$

Here A denotes the area, $c_{\alpha,\boldsymbol{k}}$ denotes the annihilation operator for the electron belonging to the flat band α at momentum $\boldsymbol{k}$ in the Moiré Brillouin zone. $\delta\rho_{\boldsymbol{q}}$ denotes the Fourier components of the density operator projected onto the flat bands with the background density at charge neutrality

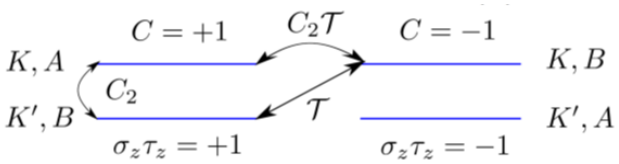

Figure 2: Schematic illustration of the Chern sectors for the flat bands in the spinless limit labelled by valley K/K' and sublattice A/B with the action of time-reversal $\mathcal{T}$, twofold rotation C_2 and the combination of the two $C_2\mathcal{T}$ illustrated

subtracted. It can be written explicitly by defining the form factor matrix

$$[\Lambda_{\boldsymbol{q}}(\boldsymbol{k})]_{\alpha,\beta} = \langle u_{\alpha,\boldsymbol{k}} | u_{\beta,\boldsymbol{k}+\boldsymbol{q}} \rangle \tag{32}$$

Here, $|u_{\alpha,\boldsymbol{k}}\rangle$ denotes the periodic Bloch wavefunctions (which differ from the Bloch wavefunctions by the factor $e^{i\boldsymbol{k}\cdot\boldsymbol{r}}$) for the flat bands.Using Λ, we can write the density operator $\rho_{\boldsymbol{q}}$ as

$$\rho_{\boldsymbol{q}} = \sum_{\alpha,\beta,\boldsymbol{k}} c^\dagger_{\alpha,\boldsymbol{k}} [\Lambda_{\boldsymbol{q}}(\boldsymbol{k})]_{\alpha,\beta} c_{\beta,\boldsymbol{k}+\boldsymbol{q}} = \sum_{\boldsymbol{k}} c^\dagger_{\boldsymbol{k}} \Lambda_{\boldsymbol{q}}(\boldsymbol{k}) c_{\boldsymbol{k}+\boldsymbol{q}}, \qquad \bar{\rho}_{\boldsymbol{q}} = \frac{1}{2} \sum_{\boldsymbol{k},\boldsymbol{G}} \delta_{\boldsymbol{q},\boldsymbol{G}} \operatorname{tr} \Lambda_{\boldsymbol{G}}(\boldsymbol{k}) \tag{33}$$

Note here that $\boldsymbol{k}$ lies in the Moiré Brilluoin zone, $\boldsymbol{q}$ is unrestricted, and $\boldsymbol{G}$ is a reciprocal lattice vector. In the second equality for $\rho_{\boldsymbol{q}}$ above, we used a more compact matrix notation where $c_{\boldsymbol{k}}$ is an 8-component column vector and $\Lambda_{\boldsymbol{q}}(\boldsymbol{k})$ is an 8×8 matrix.

Using symmetries in the chiral limit, (see Appendix B.1 for the detailed analysis), we obtain a very simple form of the form factor matrix:

$$\Lambda_{\boldsymbol{q}}(\boldsymbol{k}) = F_{\boldsymbol{q}}(\boldsymbol{k}) e^{i\Phi_{\boldsymbol{q}}(\boldsymbol{k})\sigma_z\tau_z} \tag{34}$$

where $F_{\boldsymbol{q}}(\boldsymbol{k})$ and $\Phi_{\boldsymbol{q}}(\boldsymbol{k})$ are scalars. Note that the form factor of a given flat band only depends on the combination $\sigma_z\tau_z$ which corresponds to the Chern number. This can be understood from the fact that in addition to being diagonal in spin and valley, bands in the same valley with opposite Chern number live on opposite sublattices. This leads to the form above, on further noticing that Chern number flips under exchanging sublattice (under $C_2\mathcal{T}$ symmetry), or valley (under $\mathcal{T}$) but remains invariant under flipping both (under C_2 symmetry). This illustrated in Fig. 2 where the spin degree of freedom is suppressed since it does not play a role in understanding the action of other symmetries (this arises since the problem has a full SU(2) spin rotation invariance).

The non-interacting part $h_{\alpha,\beta}(\boldsymbol{k})$ is naively obtained by projecting the chiral BM Hamiltonian onto the flat bands

$$h_{\alpha,\beta}(\boldsymbol{k}) = \langle u_{\alpha,\boldsymbol{k}} | H_{\mathrm{BM}}(\boldsymbol{k}) | u_{\beta,\boldsymbol{k}} \rangle \tag{35}$$

which suggests that it vanishes identically at the magic angle. In reality, the process of projecting onto the flat band also generates corrections coming from the interaction with the remote bands that contribute to the single particle dispersion $h_{\alpha,\beta}(\boldsymbol{k})$ [13, 9, 7]. While a detailed calculation of these corrections is beyond the scope of these notes, we can deduce the general form of $h_{\alpha,\beta}(\boldsymbol{k})$ and of the form factors $\Lambda_{\boldsymbol{q}}(\boldsymbol{k})$ based on symmetry alone. See Appendix B for a complete discussion of the symmetries of chiral TBG.

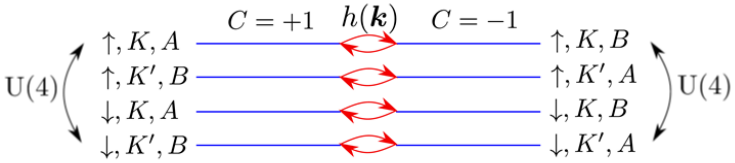

Figure 3: Illustration of the enlarged U(4) × U(4) symmetry corresponding to independent unitary rotation in each Chern sector which is reduced to U(4) in the presence of tunneling which couples the two sectors together.

3.2.1 Enlarged Symmetry

Let us now restore the spin degree of freedom and consider the symmetry of the full problem. The simple structure of the form factor implies that the interaction term in the Hamiltonian (31) has a large symmetry. To see this, we note that the density operator is invariant under any unitary rotation

$$c_{\boldsymbol{k}} \mapsto U c_{\boldsymbol{k}}, \qquad [U, \sigma_z \tau_z] = 0 \tag{36}$$

where as before $c_{\boldsymbol{k}}$ is an 8-component column vector which means that U is an 8×8 matrix. The condition that U commutes with $\sigma_z \tau_z$ simply means we restrict ourselves to unitary rotations which conserve the Chern number i.e. which take place within the same Chern sector. Since there are four band with each Chern sector ± 1. This leads to a U(4) × U(4) symmetry for the interaction term.

To see how this symmetry is reduced in the presence of the single particle term $h(\boldsymbol{k})$, we need to see how the different symmetries restrict its form. Our main assumption is that, although its value may be renormalized by interactions, it has the same symmetries as the projected chiral BM Hamiltonian (31). First, we can again use spin and valley symmetries to deduce $h(\boldsymbol{k})$ is proportional to s_0 and diagonal in valley index. For a single valley, $h(\boldsymbol{k})$ is further restricted by symmetry as described in the Appendix B.2.

This leads to the form:

$$h(\boldsymbol{k}) = h_x(\boldsymbol{k})\sigma_x + h_y(\boldsymbol{k})\sigma_y \tau_z \tag{37}$$

To understand how this term reduces the U(4) × U(4) symmetry of the interaction, it is useful to introduce a new Pauli triplet $(\gamma_x, \gamma_y, \gamma_z) = (\sigma_x, \sigma_y \tau_z, \sigma_z \tau_z)$. The condition $[U, \sigma_z \tau_z] = 0$ then becomes $[U, \gamma_z] = 0$ which yields

$$U = \begin{pmatrix} U_+ & 0 \\ 0 & U_- \end{pmatrix}_{\gamma_z} \tag{38}$$

If we want U to also commute with the single-particle part $h(\boldsymbol{k})$, we need to require $[U, \gamma_x] = 0$ in addition which gives $U_+ = U_-$, i.e. $U \propto \gamma_0$. This reduces the U(4) × U(4) of the interaction to a single U(4). Intuitively, this can be understood by noting that $h(\boldsymbol{k})$ has the form of a tunneling which connects opposite sublattice bands in the same valley (and spin) in the the opposite Chern sector. This requires us to perform the same U(4) symmetry on both sides to retain the structure of this coupling between the Chern bands thereby reducing U(4) × U(4) to a single U(4). This is schematically illustrated in Fig. 3.

Let us now briefly comment on the symmetry reduction once we move away from the chiral limit. As shown in Appendix B.3, deviation from the chiral limit means that the wavefunctions are not completely sublattice-polarized. This leads to the appearance of a sublattice off-diagonal contribution to the form factor proportional to $\sigma_x\tau_z$ and σ_y. To understand the symmetry reduction due to this extra term, it is convenient to introduce the Pauli triplet $(\eta_x, \eta_y, \eta_z) = (\sigma_x\tau_x, \sigma_x\tau_y, \tau_z)$ which commute with $\gamma_{x,y,z}$. We then find that away from the chiral limit, a unitary rotation U leaves the interaction invariant if and only if $[U, \gamma_z] = [U, \gamma_x\eta_z] = 0$. This means that U_+ and U_- defined in Eq. 38 are related via $U_+ = \eta_z U_- \eta_z$. This is different from the U(4) symmetry preserved by $h(\boldsymbol{k})$ which is given by $U_+ = U_-$. In fact, the two conditions are only satisfied if $U_+ = \eta_z U_+ \eta_z$ which corresponds to the physical symmetry group $\mathrm{U}(2) \times \mathrm{U}(2)$ which independent spin and charge conservation in each valley.

3.3 Correlated insulators: "quantum Hall ferromagnets"

We can now understand the emergence of correlated insulators at integer fillings. For simplicity, we are going to focus on the spinless limit where the interaction has a $\mathrm{U}(2) \times \mathrm{U}(2)$ symmetry which is reduced to U(2) in the presence of the single-particle dispersion. We will also focus on the case of charge neutrality. The relevance of this limit for TBG can be understood as follows. There is good experimental evidence [14, 12] for spin polarization in the vicinity of half-filling [1]. Furthermore, this spin polarization takes place at significantly higher temperature compared to those associated with the correlated insulating and superconducting phases. This suggests that the energy scale for this spin ordering (the spin stiffness) is larger than the scales associated with the correlated insulating or superconducting behavior, which justifies projecting out the completely empty/completely full spin sector and focusing on the spinless limit.

Thus, we are going to focus on the spinless model at half-filling i.e. two out of four bands are filled. Let us start by focusing on the interaction term and ignoring the single-particle dispersion. We note that the interaction is a sum of positive semidefinite operators for each momentum $\boldsymbol{q}$, thus its spectrum is non-negative. Furthermore, any state which satisfies $\delta\rho_{\boldsymbol{q}}|\Psi\rangle = 0$ for all $\boldsymbol{q}$ is a ground state for the interacting part. Let use now write the density operator more explicitly using Eqs. 33 and 57

$$\rho_{\boldsymbol{q}} = \sum_{\boldsymbol{k}} F_{\boldsymbol{q}}(\boldsymbol{k})[e^{i\Phi_{\boldsymbol{q}}(\boldsymbol{k})}(c^\dagger_{A,K,\boldsymbol{k}} c_{A,K,\boldsymbol{k}+\boldsymbol{q}} + c^\dagger_{B,K',\boldsymbol{k}} c_{B,K',\boldsymbol{k}+\boldsymbol{q}}) + e^{-i\Phi_{\boldsymbol{q}}(\boldsymbol{k})}(c^\dagger_{A,K,\boldsymbol{k}} c_{A,K,\boldsymbol{k}+\boldsymbol{q}} + c^\dagger_{B,K',\boldsymbol{k}} c_{B,K',\boldsymbol{k}+\boldsymbol{q}})] \tag{39}$$

We see that $\rho_{\boldsymbol{q}}$ consists of four terms which correspond to a momentum space hopping between $\boldsymbol{k}$ and $\boldsymbol{k}+\boldsymbol{q}$ in each of the four bands seperately. Thus, the four terms are gauranteed to vanish if they act on a state where each of the four bands is completely empty or completely full yielding a ground state of the interacting Hamiltonian.[2]

This yields two possible kinds of ground states at half-filling (2 out of 4). First, we can fill two

[1] Note that due to the presence of SU(2) spin rotation symmetry in each valley separately, a spin polarized state does not have to be a ferromagnet since we can choose the filled spin independently in each valley.

[2] This is only valid if $\boldsymbol{q}$ is not equal to a reciprocal lattice vector $\boldsymbol{G}$ which yields a term $c^\dagger_{\boldsymbol{k}} c_{\boldsymbol{k}+\boldsymbol{G}} = c^\dagger_{\boldsymbol{k}} c_{\boldsymbol{k}}$ that is equal to the filling of electrons at momentum $\boldsymbol{k}$. This term yields a constant which cancels against the background term $\bar{\rho}_{\boldsymbol{q}}$ in $\delta\rho_{\boldsymbol{q}}$ such that $\delta\rho_{\boldsymbol{q}}|\Psi\rangle = 0$ for all $\boldsymbol{q}$.

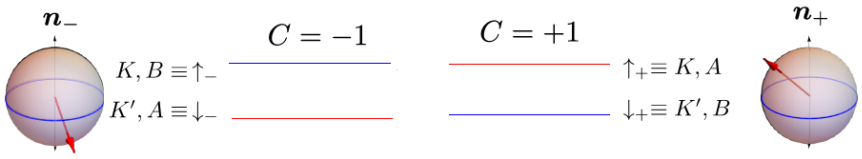

Figure 4: Illustration of the Pseudospin vector with K, A and K, B denoting the up pseudospin direction in the $\pm$ Chern sectors, respectively

bands in the same Chern sector yields an anomalous quantum Hall state

$$|\Psi_{\text{QAH},+2}\rangle = \prod_{\boldsymbol{k}\in\text{mBZ}} c^\dagger_{A,K,\boldsymbol{k}} c^\dagger_{B,K',\boldsymbol{k}}|0\rangle, \qquad |\Psi_{\text{QAH},-2}\rangle = \prod_{\boldsymbol{k}\in\text{mBZ}} c^\dagger_{B,K,\boldsymbol{k}} c^\dagger_{A,K',\boldsymbol{k}}|0\rangle \tag{40}$$

$|\Psi_{\text{QAH},\pm 2}\rangle$ has Chern number ± 2 and map to each other under time-reversal symmetry $\mathcal{T}$ i.e. each of them spontaneously breaks $\mathcal{T}$. Both states are symmetric under the $\text{U}(2)\times\text{U}(2)$ symmetry since unitary rotations among two fully filled or fully empty bands does nothing. The second class of states is obtained by filling one band in each of the $\pm$ Chern sectors leading to a vanishing total Chern number. This can be chosen to be any arbitrary linear combination of the two bands in each Chern sector yielding the state

$$|\Psi_{\theta_+,\phi_+,\theta_-,\phi_-}\rangle = \prod_{\boldsymbol{k}\in\text{mBZ}} (\cos\theta_+ c^\dagger_{A,K,\boldsymbol{k}} + \sin\theta_+ e^{i\phi_+} c^\dagger_{B,K',\boldsymbol{k}})(\cos\theta_- c^\dagger_{B,K,\boldsymbol{k}} + \sin\theta_- e^{i\phi_-} c_{A,K',\boldsymbol{k}})|0\rangle \tag{41}$$

The angles $\theta_\pm$ and $\phi_\pm$ parametrize two unit vectors $\boldsymbol{n}_\pm = (\sin\theta_\pm\cos\phi_\pm, \sin\theta_\pm\sin\phi_\pm, \cos\theta_\pm)$. Another way to see this is to start from a simple state, let's say $\theta_\pm = 0$, corresponding to a valley polarized state filling both sublattice bands in the K valley. Since a single band out of 2 is selected to be filled in each Chern sector, this state breaks the $\text{U}(2)\times\text{U}(2)$ symmetry of the interaction. For each Chern sector, the U(2) symmetry is broken down to $\text{U}(1)\times\text{U}(1)$ corresponding to independent phase rotation in the full or empty band. Thus, acting with $\text{U}(2)\times\text{U}(2)$ on the valley polarized state generates a manifold of states characterized by a unit vector in $S^2 = \frac{\text{U}(2)}{\text{U}(1)\times\text{U}(1)}$ in each of the two Chern sectors.

We will call the two unit vectors $\boldsymbol{n}_+$ and $\boldsymbol{n}_-$ parametrizing the manifold of Chern zero states pseudospins (see Fig. 4). These can be extracted from the ground state wavefunction by introducing the pseudospin Pauli triplet $(\eta_x, \eta_y, \eta_z) = (\sigma_x\tau_x, \sigma_x\tau_y, \tau_z)$ via

$$\boldsymbol{n}_\pm = \langle\Psi|\boldsymbol{\eta}\frac{1\pm\gamma_z}{2}|\Psi\rangle \tag{42}$$

It is instructive to look at some special points on this manifold which are invariant under some physical symmetries. First, we notice that the U(1) valley rotation associated with the conservation of the valley charge acts as a pseudospin rotation in the x-y plane $e^{i\phi\tau_z} = e^{i\phi\eta_z}$. Thus, if both the pseudospins $\boldsymbol{n}_\pm$ point in the z-direction, the resulting state would preserve U(1) valley symmetry. There are two options, either $\boldsymbol{n}_+ = \boldsymbol{n}_- = \pm\hat{z}$ corresponding to aligned Ising order between the Chern sectors or $\boldsymbol{n}_+ = -\boldsymbol{n}_- = \pm\hat{z}$ corresponding to anti-aligned Ising order between the Chern sector. The former corresponds $\langle\tau_z\rangle \neq 0$ and is obtained by filling the same valley in the two Chern sectors (both sublattice bands in the same valley) leading to a valley polarized state which is invariant under $C_2\mathcal{T}$ (remember $C_2\mathcal{T}$ flips sublattice but not valley). The latter corresponds

to $\langle\sigma_z\rangle \neq 0$ and is obtained by filling opposite valleys for the two different Chern sectors (or equivalently filling both valleys in only one of the sublattices) leading to a valley Hall state which is invariant under time-reversal symmetry (remember $\mathcal{T}$ flips valley but not sublattice). In-plane pseudospin order spontaneously breaks U(1) valley symmetry, but we can still distinguish two cases of XY pseudospin order which is aligned or anti-aligned between the Chern sector. The aligned case corresponds to a non-vanishing expectation value for the order parameter $\langle\sigma_x\tau_{x,y}\rangle = \langle\eta_{x,y}\rangle \neq 0$ which is invariant under time-reversal symmetry whereas the anti-aligned case corresponds to the order parameter $\langle\sigma_y\tau_{x,y}\rangle = \langle\gamma_z\eta_{x,y}\rangle \neq 0$ which is odd under time-reversal, but invariant under a combination of time-reversal and π valley rotation. Since $\mathcal{T}$ anticommutes with τ_z (it exchanges valleys), the combination $\mathcal{T}' = i\tau_z\mathcal{T}$ acts as a new time-reversal symmetry which squares to -1 rather than $+1$, i.e. a Kramers type time-reversal symmetry. A summary of these states is given below in Table 2.

State	Pseudospin Description	Unbroken Symmetries
Valley Polarized τ_z	Ising Aligned η_z	$\mathrm{U}_V(1), C_2\mathcal{T}$
Valley Hall σ_z	Ising Anti-aligned $\gamma_z\eta_z$	$\mathrm{U}_V(1), \mathcal{T}$
$\mathcal{T}$-symmetric Intervalley $\sigma_x\tau_{x,y}$	XY Aligned $\eta_{x,y}$	$\mathcal{T}$
Kramers Intervalley $\sigma_y\tau_{x,y}$	XY Anti-aligned $\gamma_z\eta_{x,y}$	$\mathcal{T}' = i\tau_z\mathcal{T}$

Table 2: Table summarizing some of the states from the manifold of the Chern zero low-energy states, their corresponding pseudospin description, and their symmetries. The pseudospin order is ferromagnetic within each Chern sector but it can be aligned $\boldsymbol{n}_+ = \boldsymbol{n}_-$ or anti-aligned $\boldsymbol{n}_+ = -\boldsymbol{n}_-$ between Chern sectors.

3.3.1 Effect of dispersion

The analysis of the ground state so far focused on the ground states of the interacting term ignoring the single-particle dispersion $h(\boldsymbol{k})$. As discussed earlier, this term is likely to be non-zero even for the chiral limit at the magic angle and has the general form given by (37) which breaks the $\mathrm{U}(2)\times\mathrm{U}(2)$ symmetry down to a single U(2). Our main assumption here is that the magnitude of this term is small compared to the interaction scale such that its effect can be included perturbatively leading to a splitting among the ground states of the interaction part.

Before computing this splitting, we will present a simple intuitive argument to understand the effect of this term. h acts as tunneling between opposite Chern (sublattice) bands belonging to the same valley. If we are in a state where both these bands are fully filled or fully empty e.g. in a valley polarized state, then this tunneling term is Pauli blocked and has no effect on the energy of the state. On the other hand, if one band is fully filled and the other is fully empty, this tunneling term is expected to reduce the energy through virtual tunneling. This reduction mechanism is analogous to superexchange and leads to an energy reduction of the order of h^2/U where U is the interaction scale.

For a state in the manifold of zero Chern insulators described by the pseudospin vectors $\boldsymbol{n}_+$ and $\boldsymbol{n}_-$, the energy correction due to tunneling can only be a function of $\boldsymbol{n}_+\cdot\boldsymbol{n}_-$ due to SU(2) pseudospin symmetry. Furthermore, if we compute this contribution in second order perturbation theory it can only depend linearly on $\boldsymbol{n}_+\cdot\boldsymbol{n}_-$ leading to the energy contribution $\Delta E = J(\boldsymbol{n}_+\cdot\boldsymbol{n}_- - 1)$ where we have added an unimportant constant such that ΔE vanishes for $\boldsymbol{n}_+ = \boldsymbol{n}_-$ as expected. The

value of J can be computed by taking any of the states with $\boldsymbol{n}_+ = -\boldsymbol{n}_-$ for which $\Delta E = -2J$. For definiteness, let us take the valley Hall state with $\boldsymbol{n}_+ = -\boldsymbol{n}_- = \hat{z}$. Relegating technical details to appendix C, we can extract the value of J by computing the second order correction to the energy due to h leading to

$$J = \frac{1}{N}\sum_{\boldsymbol{k},\boldsymbol{k}'}[h_x(\boldsymbol{k}) + ih_y(\boldsymbol{k})][\mathcal{H}_{\text{eh}}]^{-1}_{\boldsymbol{k},\boldsymbol{k}'}[h_x(\boldsymbol{k}) - ih_y(\boldsymbol{k})], \tag{43}$$

where $\mathcal{H}_{\text{eh}}$ is the Hamiltonian for an interChern particle-hole excitation created by the action of $h(\boldsymbol{k})$. Its explicit form is given by [2]

$$[\mathcal{H}_{\text{eh}}]_{\boldsymbol{k},\boldsymbol{k}'} = \frac{1}{A}\sum_{\boldsymbol{q}} V_{\boldsymbol{q}} F_{\boldsymbol{q}}(\boldsymbol{k})^2[\delta_{\boldsymbol{k},\boldsymbol{k}'} - \delta_{\boldsymbol{k}',[\boldsymbol{k}+\boldsymbol{q}]}e^{2i\Phi_{\boldsymbol{q}}(\boldsymbol{k})}] \tag{44}$$

where $[\boldsymbol{q}]$ denotes the part of $\boldsymbol{q}$ within the first Moiré Brillouin zone. As discussed in Ref. [2], this Hamiltonian always has a finite spectral gap due to the topological properties of the bands which guarantees that the perturbation theory is well-defined.

3.3.2 Deviation from the chiral limit

Let us now see how the deviation from the chiral limit influences the energies of the states in the ground state manifold. We start by noting, away from the chiral limit, the wavefunctions are not completely sublattice-polarized leading to sublattice off-diagonal contribution to the form factor matrix proportional to $\sigma_x\tau_z$ and σ_y (see appendix B.3 for details). The extra sublattice off-diagonal contribution to the form factor means that the density operator has a corresponding extra term given by

$$\begin{aligned}\tilde{\rho}_{\boldsymbol{q}} &= \sum_{\boldsymbol{k}} \tilde{F}_{\boldsymbol{q}}(\boldsymbol{k}) c^\dagger_{\boldsymbol{k}}\sigma_x\tau_z e^{i\tilde{\Phi}_{\boldsymbol{q}}(\boldsymbol{k})\sigma_z\tau_z} c_{\boldsymbol{k}+\boldsymbol{q}} \\ &= \sum_{\boldsymbol{k}} \tilde{F}_{\boldsymbol{q}}(\boldsymbol{k})[e^{-i\tilde{\Phi}_{\boldsymbol{q}}(\boldsymbol{k})}(c^\dagger_{A,K,\boldsymbol{k}}c_{B,K,\boldsymbol{k}+\boldsymbol{q}} - c^\dagger_{B,K',\boldsymbol{k}}c_{A,K',\boldsymbol{k}+\boldsymbol{q}}) + e^{i\tilde{\Phi}_{\boldsymbol{q}}(\boldsymbol{k})}(c^\dagger_{B,K,\boldsymbol{k}}c_{A,K,\boldsymbol{k}+\boldsymbol{q}} - c^\dagger_{A,K',\boldsymbol{k}}c_{B,K',\boldsymbol{k}+\boldsymbol{q}})]\end{aligned} \tag{45}$$

This represents hopping between opposite sublattices within the same valley. Including this term, we find that the condition that a state is a ground state for the full interaction term is $\delta\rho_{\boldsymbol{q}}|\Psi\rangle = \tilde{\rho}_{\boldsymbol{q}}|\Psi\rangle = 0$ for all $\boldsymbol{q}$. This is manifestly satisfied by the valley polarized state, but it is also satisfied by the Kramers intervalley coherent state which is generated from the valley polarized state by unitary rotations generated by $\gamma_z\eta_{x,y}$. In fact, we can deduce the form of the energy contribution due to deviation from the chiral limit based on symmetry considerations alone since invariance under the SU(2) group generated by $\eta_x\gamma_z$, $\eta_y\gamma_z$, and η_z restricts the energy to the form

$$\Delta E = \lambda(n_{+,x}n_{-,x} + n_{+,y}n_{-,y} - n_{+,z}n_{-,z} + 1) \tag{46}$$

where we added a constant such that ΔE vanishes for the valley polarized state as expected. The value of λ can be deduced by taking a state which maximizes ΔE, e.g. valley Hall state with $\Delta E = 2\lambda$. A direct calculation yields

$$\lambda = \frac{1}{4A}\sum_{\boldsymbol{q}} V_{\boldsymbol{q}}\langle\Psi_{\text{VH}}|\tilde{\rho}_{\boldsymbol{q}}\tilde{\rho}_{-\boldsymbol{q}}|\Psi_{\text{VH}}\rangle = \frac{1}{2A}\sum_{\boldsymbol{q}} V_{\boldsymbol{q}}\tilde{F}_{\boldsymbol{q}}(\boldsymbol{k})^2 \tag{47}$$

3.3.3 Energy splitting

Combining the effects of the dispersion and deviation from the chiral limit yields the following energy function for the splitting

$$\Delta E[\boldsymbol{n}_+, \boldsymbol{n}_-] = J\boldsymbol{n}_+ \cdot \boldsymbol{n}_- + \lambda(\boldsymbol{n}_{+,xy} \cdot \boldsymbol{n}_{-,xy} - n_{+,z}n_{-,z}) \tag{48}$$

This function selects the anti-aligned XY order (the Kramers intervalley coherent state) as the unique ground state.

A Landau Levels of Graphene and Projected Density Operators

In this appendix, let us briefly review the effect of a magnetic field on the electronic structure near graphene's neutrality point. Consider the K valley and note that setting $\hbar = v_F = 1$ we can write $H_+ = -2i\sigma^+\partial_z + \text{h.c.}$, where $z = x + iy$, $2\partial_z = \partial_x - i\partial_y$. Now, coupling a uniform magnetic field in the circular gauge $A_i = -\frac{B}{2}\epsilon_{ij}x_j$, we have the effective Hamiltonian:

$$H_+ = -2i\sigma^+\left(\partial_z - \frac{\bar{z}}{4l_B^2}\right) - 2i\sigma^-\left(\partial_{\bar{z}} + \frac{z}{4l_B^2}\right) \tag{49}$$

We can find a family of zero mode eigenstates as follows. First note the spinor: $\psi_0 = \begin{bmatrix} e^{-z\bar{z}/4l_B^2} \\ 0 \end{bmatrix}$ is a zero mode so $H_+\psi_0 = 0$. Next, any arbitrary analytic function $f(z)$ multiplying this spinor also gives a zero mode; $\psi = f(z)\psi_0$, $H_+\psi = 0$. These are nothing but the zeroth Landau levels of graphene. The wavefunctions in the other valley can be obtained by performing a C_2 rotation. Note the states live entirely on one sublattice in one valley, and on the opposite sublattice in the opposite valley. This ends up leading to an approximate SU(4) symmetry for electrons with spin degeneracy since the density operator can be written as: $\rho = \rho_{K\uparrow} + \rho_{K\downarrow} + \rho_{K'\uparrow} + \rho_{K'\downarrow}$, where the density operator $\rho(r) = \sum_{\sigma=\uparrow,\downarrow} c_\sigma^\dagger(r)c_\sigma(r)$ is projected into the lowest Landau level.

Let us also mention the effect of projecting the density operator into the lowest Landau level. For this purpose it will be helpful to consider the first quantized density operator: $\rho(q) = e^{iq\cdot r}$. In the lowest Landau level we can separate $\mathbf{r} = \mathbf{R} + i\frac{l_B^2}{2}\hat{z} \times \Pi$, where R is the guiding center coordinate which remains unconstrained in the lowest landau level, while the momentum $\Pi = (-i\nabla - \frac{1}{2l_B^2}\hat{z}\times r)$ accounts for the cyclotron orbits. The Hamiltonian is written as $H_+ = \Pi_x\sigma_x + \Pi_y\sigma_y$. The guiding center coordinates can be written as $\mathbf{R} = \mathbf{r} - l_B^2\hat{z} \times \Pi$. The only nonvanishing commutators are $[\Pi_x, \Pi_y] = il_B^{-2}$; $[R_x, R_y] = -il_B^2$. Defining raising and lowering operators $b^\dagger = \frac{l_B}{\sqrt{2}}(\Pi_x - i\Pi_y)$ and $a^\dagger = \frac{1}{\sqrt{2}l_B}(R_x + iR_y)$.

Thus we have: $\rho(q) = e^{i\mathbf{q}\cdot\mathbf{r}}$ where $\mathbf{q}\cdot\mathbf{r} = \frac{l_B}{\sqrt{2}}(\bar{q}a^\dagger + qa) - i\frac{l_B}{\sqrt{2}}(qb^\dagger - \bar{q}b)$. Projecting into the lowest landau level and measuring all q in units of l_B, i.e. using the dimensionless $Q = ql_B$, we have: $\rho_Q = e^{-Q^2/4}\tilde{\rho}_Q$, where $\tilde{\rho}_Q = e^{\frac{i}{\sqrt{2}}(Qa+\bar{Q}a^\dagger)}$. This readily gives us the algebra:

$$\tilde{\rho}_Q\tilde{\rho}_{Q'} = e^{\frac{i}{2}Q\wedge Q'}\tilde{\rho}_{Q+Q'} \tag{50}$$

where $Q \wedge Q' = \hat{\mathbf{z}} \cdot \mathbf{Q} \times \mathbf{Q}'$.

B Symmetries of the chiral model

The main feature of the chiral TBG Hamiltonian is the presence of a chiral or sublattice symmetry which anticommutes with the single-particle Hamiltonian $\{\sigma_z, H\} = 0$. In addition, weak-spin orbit coupling in graphene implies that H is invariant under SU(2) spin rotations, i.e. $H \propto s_0$. The large momentum separation between the graphene valleys leads to valley decoupling at low energies relevant to TBG physics which implies independent spin and charge conservation in each valley i.e. H is diagonal in the valley index τ_z. The two valley are related by spinless time-reversal symmetry which is implemented as $\mathcal{T} = \tau_x \mathcal{K}$ with $\mathcal{K}$ denoting complex conjugation, such that $H_{K'}(\boldsymbol{k}) = H_K(-\boldsymbol{k})^*$. The single particle Hamiltonian is also invariant under two-fold rotation symmetry which flips sublattice and valley $C_2 = \sigma_x \tau_x$. The combination of the two $C_2\mathcal{T} = \sigma_x \mathcal{K}$ leaves the valley index invariant and relates the two sublattice wavefunctions at the same momentum $\boldsymbol{k}$.

A more subtle symmetry of the chiral TBG Hamiltonian is a particle-hole symmetry $H(-\boldsymbol{k})^* = \mu_y \sigma_x H(\boldsymbol{k}) \mu_y \sigma_x$ where μ denote the Pauli matrices in layer space [10, 5]. On the level of the single-particle Hamiltonian this is an antiunitary anticommuting symmetry given by $\mathcal{P} = i\mu_y \sigma_x \mathcal{K}$ whereas in second quantized language, this is a unitary particle-hole symmetry acting as

$$\mathcal{P}^{-1} f_{\boldsymbol{k}} \mathcal{P} = \mu_y \sigma_x f^\dagger_{-\boldsymbol{k}}, \qquad \mathcal{P}^{-1} i \mathcal{P} = i \tag{51}$$

where $f_{\boldsymbol{k}}$ denotes the annihilation operators for microscopic electrons. In addition to the sublattice, valley, and spin indices, these electrons also carry a layer index.

Since the chiral symmetry σ_z is anticommuting and unitary (anti-unitary particle-hole in second quantization), $\mathcal{T}$ is commuting and anti-unitary (anti-unitary in second quantization), and $\mathcal{P}$ is anti-commuting and anti-unitary (unitary particle-hole in second quantization), their product $R = i\sigma_z \mathcal{P}\mathcal{T} = \tau_x \sigma_y \mu_y$ is a Z_2 unitary commuting symmetry. This extra "hidden" symmetry relates different valley, sublattice and layer indices and leads to enhanced symmetry of the interacting problem as we will see below.

B.1 Symmetries and the Form Factor

Let us now see how that symmetries restrict the structure of the form factor $\Lambda_{\boldsymbol{q}}(\boldsymbol{k})$. Due to the SU(2) spin rotation symmetry, the spin index does not play any role in the following discussion so it can be dropped. This essentially corresponds to considering a spinless version of the problem. In the following, we will write out the flat band index α in terms of the sublattice-valley indices σ and τ. We note that sublattice symmetry implies that $\Lambda_{\boldsymbol{q}}(\boldsymbol{k})$ is diagonal in the sublattice index since

$$\langle u_{A,\tau,\boldsymbol{k}} | u_{B,\tau,\boldsymbol{k}'} \rangle = \langle u_{A,\tau,\boldsymbol{k}} | \sigma_z^2 | u_{B,\tau,\boldsymbol{k}'} \rangle = -\langle u_{A,\tau,\boldsymbol{k}} | u_{B,\tau,\boldsymbol{k}'} \rangle = 0 \tag{52}$$

where we used $\sigma_z |u_{A/B,\tau,\boldsymbol{k}'}\rangle = \pm |u_{A/B,\tau,\boldsymbol{k}'}\rangle$. In addition, valley symmetry implies that $\Lambda_{\boldsymbol{q}}(\boldsymbol{k})$ is also diagonal in valley. We now note that since $C_2\mathcal{T}$ flips sublattice but not momentum, its action can be written as

$$C_2 \mathcal{T} u_{\sigma,\tau,\boldsymbol{k}} = e^{i\eta_{\sigma,\tau,\boldsymbol{k}}} u^*_{-\sigma,\tau,\boldsymbol{k}} \tag{53}$$

Since we are free to choose the gauge independently in the two valleys $\tau = \pm = K/K'$ and sublattices $\sigma = \pm = A/B$, we can set $\eta_{\sigma,\tau,\boldsymbol{k}}$ by fixing the gauge in sublattice B relative to A. This

means that $C_2\mathcal{T}$ acts as $\sigma_x\mathcal{K}$ in the flat band basis. Next, we note that since R symmetry flips both valley and sublattice, we have

$$Ru_{\sigma,\tau,\boldsymbol{k}} = e^{i\phi_{\sigma,\tau,\boldsymbol{k}}}u_{-\sigma,-\tau,\boldsymbol{k}} \tag{54}$$

Here, we are also free to make a gauge choice to get rid of the phases $\phi_{\sigma,\tau,\boldsymbol{k}}$. This means that the action of any of the remaining symmetries, e.g. $\mathcal{T}$ or C_2, on the flat band will contain extra phase factors that cannot be removed. In particular, it can be shown that the band topology enforces a non-trivial phase factors for C_2 symmetry.

Using Eq. 54, we can relate the diagonal entries of the form factor between σ, τ and $-\sigma, -\tau$

$$\langle u_{\sigma,\tau,\boldsymbol{k}}|u_{\sigma,\tau,\boldsymbol{k}+\boldsymbol{q}}\rangle = \langle u_{\sigma,\tau,\boldsymbol{k}}|R^2|u_{\sigma,\tau,\boldsymbol{k}+\boldsymbol{q}}\rangle = \langle u_{-\sigma,-\tau,\boldsymbol{k}}|u_{-\sigma,-\tau,\boldsymbol{k}+\boldsymbol{q}}\rangle \tag{55}$$

This can be used to relate the form factors in opposite valleys at the same momentum. In addition, we can use Eq. 53 to related the form factors within the same valley for the two sublattices leading to

$$\langle u_{\sigma,\tau,\boldsymbol{k}}|u_{\sigma,\tau,\boldsymbol{k}+\boldsymbol{q}}\rangle = \langle u_{\sigma,\tau,\boldsymbol{k}}|(C_2\mathcal{T})^2|u_{\sigma,\tau,\boldsymbol{k}+\boldsymbol{q}}\rangle = \langle u_{-\sigma,\tau,\boldsymbol{k}}|u_{-\sigma,\tau,\boldsymbol{k}+\boldsymbol{q}}\rangle^* \tag{56}$$

Thus, the diagonal entries of the form factor are related by complex conjugation upon exchanging sublattice or valley but remain the same under exchanging both. This leads to the following simple form of the form factor matrix

$$\Lambda_{\boldsymbol{q}}(\boldsymbol{k}) = F_{\boldsymbol{q}}(\boldsymbol{k})e^{i\Phi_{\boldsymbol{q}}(\boldsymbol{k})\sigma_z\tau_z} \tag{57}$$

where $F_{\boldsymbol{q}}(\boldsymbol{k})$ and $\Phi_{\boldsymbol{q}}(\boldsymbol{k})$ are scalars. Note that the form factor of a given flat band only depends on the combination $\sigma_z\tau_z$ which corresponds to the Chern number. This flips under exchanging sublattice (under $C_2\mathcal{T}$ symmetry), or valley (under $\mathcal{T}$) but remains invariant under flipping both (under C_2 symmetry).

B.2 Symmetries and the Kinetic Term

Different symmetries restrict the form of the single particle term $h(\boldsymbol{k})$. Our main assumption is that, although its value may be renormalized by interactions, it has the same symmetries as the projected chiral BM Hamiltonian (31). First, we can again use spin and valley symmetries to deduce $h(\boldsymbol{k})$ is proportional to s_0 and diagonal in valley index. For a single valley, $h(\boldsymbol{k})$ is stricly off-diagonal in sublattice index since:

$$\langle u_{\sigma,\tau,\boldsymbol{k}}|H_{\mathrm{BM}}(\boldsymbol{k})|u_{\sigma,\tau,\boldsymbol{k}}\rangle = -\langle u_{\sigma,\tau,\boldsymbol{k}}|\sigma_z H_{\mathrm{BM}}(\boldsymbol{k})\sigma_z|u_{\sigma,\tau,\boldsymbol{k}}\rangle = -\langle u_{\sigma,\tau,\boldsymbol{k}}|H_{\mathrm{BM}}(\boldsymbol{k})|u_{\sigma,\tau,\boldsymbol{k}}\rangle = 0 \tag{58}$$

This means that the matrix $h(\boldsymbol{k})$ can only contain the terms $\sigma_x, \sigma_y, \sigma_x\tau_z$, and $\sigma_y\tau_z$. We can use the R symmetry to restrict this form further using

$$\langle u_{\sigma,\tau,\boldsymbol{k}}|H_{\mathrm{BM}}(\boldsymbol{k})|u_{\sigma',\tau',\boldsymbol{k}}\rangle = \langle u_{\sigma,\tau,\boldsymbol{k}}|RH_{\mathrm{BM}}(\boldsymbol{k})R|u_{\sigma',\tau',\boldsymbol{k}}\rangle = \langle u_{-\sigma,-\tau,\boldsymbol{k}}|H_{\mathrm{BM}}(\boldsymbol{k})|u_{-\sigma',-\tau',\boldsymbol{k}}\rangle \tag{59}$$

which implies that $h(\boldsymbol{k})$ commutes with $\sigma_x\tau_x$ excluding the terms σ_y and $\sigma_x\tau_z$. This leads to the form

$$h(\boldsymbol{k}) = h_x(\boldsymbol{k})\sigma_x + h_y(\boldsymbol{k})\sigma_y\tau_z \tag{60}$$

B.3 Deviations from the chiral limit

Let us now consider what happens when we deviate from the chiral limit $w_0 = 0$. In this case, chiral symmetry is broken which means that the unitary symmetry R is also broken. As a result, we do not expect the form factors to be diagonal in the sublattice index since the wavefunctions are no longer completely sublattice polarized. We can still use valley and spin symmetries to show that the form factor is diagonal in valley and proportional to the identity in spin space.

To restrict the form factor further, we note that the particle-hole symmetry $\mathcal{P}$ remains a symmetry to a good approximation provided we assume the angle is small [3]. We note that the product of $\mathcal{P}$ and $\mathcal{T}$ anticommutes with the single particle Hamiltonian which means that the action of $\mathcal{PT} = \mu_y \tau_x \sigma_x$ maps positive energy states to negative energy states at the same momentum $\boldsymbol{k}$. As a result, it leave the space of flat bands invariant and we can write

$$\mathcal{PT} u_{\sigma,\tau,\boldsymbol{k}} = e^{i\varphi_{\sigma,\tau,\boldsymbol{k}}} u_{-\sigma,-\tau,\boldsymbol{k}} \tag{61}$$

To be compatible with the gauge choice in Appendix B.1, we choose the gauge such that $\mathcal{PT} = i\sigma_z R = \sigma_y \tau_x$ which implies that the form factor satisfies $\sigma_y \tau_x \Lambda_{\boldsymbol{q}}(\boldsymbol{k}) \sigma_y \tau_x = \Lambda_{\boldsymbol{q}}(\boldsymbol{k})$. This restricts the form factor to the terms $\tau_0 \sigma_{0,y}$ and $\tau_z \sigma_{x,z}$. In addition, we can use $C_2\mathcal{T}$ (cf. Eq. 53) to get

$$\langle u_{\sigma,\tau,\boldsymbol{k}} | u_{\sigma',\tau,\boldsymbol{k}+\boldsymbol{q}} \rangle = \langle u_{\sigma,\tau,\boldsymbol{k}} | (C_2\mathcal{T})^2 | u_{\sigma',\tau,\boldsymbol{k}+\boldsymbol{q}} \rangle = \langle u_{-\sigma,\tau,\boldsymbol{k}} | u_{-\sigma',\tau,\boldsymbol{k}+\boldsymbol{q}} \rangle^* \tag{62}$$

which yields $\Lambda_{\boldsymbol{q}}(\boldsymbol{k}) = \sigma_x \Lambda_{\boldsymbol{q}}(\boldsymbol{k})^* \sigma_x$ which implies that the coefficients of $\tau_0\sigma_0$, $\tau_0\sigma_x$ and $\tau_z\sigma_y$ are real while the coefficient of $\tau_z\sigma_z$ is imaginary leading to the form

$$\Lambda_{\boldsymbol{q}}(\boldsymbol{k}) = F_{\boldsymbol{q}}(\boldsymbol{k}) e^{i\Phi_{\boldsymbol{q}}(\boldsymbol{k})\sigma_z\tau_z} + \sigma_x\tau_z \tilde{F}_{\boldsymbol{q}}(\boldsymbol{k}) e^{i\tilde{\Phi}_{\boldsymbol{q}}(\boldsymbol{k})\sigma_z\tau_z} \tag{63}$$

Compared to Eq. 57, there is an extra sublattice off-diagonal term which is only non-vanishing away from the chiral limit.

C Perturbative correction to energy due to single-particle disperison h

To compute the perturbative correction to energy due to single-particle disperison h, we write $\Delta E = J(\boldsymbol{n}_+ \cdot \boldsymbol{n}_- - 1)$ and take $\boldsymbol{n}_+ = -\boldsymbol{n}_- = \hat{z}$. We see that the contribution from the tunneling ΔE is equal to twice the contribution from tunneling connecting a single fully filled Chern band to a single fully empty band in the opposite Chern sector. This means we can restrict ourselves to a pair of tunnel-coupled opposite Chern bands and just multiply the result by 2 [4]. For definiteness, we take the positive Chern band to be fully filled and the negative Chern band to be fully empty such that the total number of electrons in the $\pm$ band is $N_+ = N$ and $N_- = 0$. The single particle "tunneling" term has the form

$$\hat{h} = \sum_{\boldsymbol{k}} c^\dagger_{\boldsymbol{k}} h(\boldsymbol{k}) c_{\boldsymbol{k}} = \sum_{\boldsymbol{k}} c^\dagger_{+,\boldsymbol{k}} [h_x(\boldsymbol{k}) - i h_y(\boldsymbol{k})] c_{-,\boldsymbol{k}} + \text{h.c.} \tag{64}$$

[3] it is only a symmetry if we ignore the angular rotation in the Pauli matrices in Eq. **??** which is equivalent to the replacemntsuch that $\sigma_{\pm\theta/2} \mapsto \sigma$

[4] the factor of 2 cancels out due to our definition of J with $\Delta E = -2J$ such that the absolute value of the result is precisely J

where $c_{\boldsymbol{k}} = (c_{+,\boldsymbol{k}}, c_{-,\boldsymbol{k}})$ is a 2-component vector with annihilation operators in the $\pm$ Chern band. $\hat{h}$ does not conserve the particle number in each Chern sector separately. Acting with in on a state with $(N_+, N_-) = (N, 0)$ yields a state with $(N_+, N_-) = (N-1, 1)$ with an electron hole pair at some momentum $\boldsymbol{k}$ which can be written as

$$|\Psi_{\boldsymbol{k}}\rangle = c^{\dagger}_{-,\boldsymbol{k}} c_{+,\boldsymbol{k}} |\Psi_0\rangle \tag{65}$$

The interacting part of the Hamiltonian conserves momentum and Chern number so it maps the state $|\Psi_{\boldsymbol{k}}\rangle$ to a state $|\Psi_{\boldsymbol{k}'}\rangle$ and it determines the energy spectrum of the particle-hole excitations. As a result, the second order correction to the energy can be written as

$$\Delta E = -\frac{1}{N} \sum_{\boldsymbol{k},\boldsymbol{k}'} [h_x(\boldsymbol{k}) + i h_y(\boldsymbol{k})] [\mathcal{H}_{\text{eh}}]^{-1}_{\boldsymbol{k},\boldsymbol{k}'} [h_x(\boldsymbol{k}) - i h_y(\boldsymbol{k})], \tag{66}$$

with $\mathcal{H}_{\text{eh}}$ given by [2]

$$[\mathcal{H}_{\text{eh}}]_{\boldsymbol{k},\boldsymbol{k}'} = \frac{1}{2A} \sum_{\boldsymbol{q}} V_{\boldsymbol{q}} \langle \Psi_{\boldsymbol{k}} | \delta\rho_{\boldsymbol{q}} \delta\rho_{-\boldsymbol{q}} | \Psi_{\boldsymbol{k}'} \rangle = \frac{1}{A} \sum_{\boldsymbol{q}} V_{\boldsymbol{q}} F_{\boldsymbol{q}}(\boldsymbol{k})^2 [\delta_{\boldsymbol{k},\boldsymbol{k}'} - \delta_{\boldsymbol{k}',[\boldsymbol{k}+\boldsymbol{q}]} e^{2i\Phi_{\boldsymbol{q}}(\boldsymbol{k})}] \tag{67}$$

where $[\boldsymbol{q}]$ denotes the part of $\boldsymbol{q}$ within the first Moiré Brillouin zone.

References

[1] Rafi Bistritzer and Allan H. MacDonald. Moiré bands in twisted double-layer graphene. *Proceedings of the National Academy of Sciences*, 108(30):12233–12237, 2011.

[2] Nick Bultinck, Eslam Khalaf, Shang Liu, Shubhayu Chatterjee, Ashvin Vishwanath, and Michael P. Zaletel. Ground State and Hidden Symmetry of Magic Angle Graphene at Even Integer Filling. *arXiv e-prints*, page arXiv:1911.02045, Nov 2019.

[3] Stephen Carr, Shiang Fang, Ziyan Zhu, and Efthimios Kaxiras. Minimal model for low-energy electronic states of twisted bilayer graphene. *arXiv e-prints*, page arXiv:1901.03420, Jan 2019.

[4] Steven M Girvin. The quantum hall effect: novel excitations and broken symmetries. In *Aspects topologiques de la physique en basse dimension. Topological aspects of low dimensional systems*, pages 53–175. Springer, 1999.

[5] Kasra Hejazi, Chunxiao Liu, Hassan Shapourian, Xiao Chen, and Leon Balents. Multiple topological transitions in twisted bilayer graphene near the first magic angle. *Phys. Rev. B*, 99:035111, Jan 2019.

[6] Patrick J. Ledwith, Grigory Tarnopolsky, Eslam Khalaf, and Ashvin Vishwanath. Fractional chern insulator states in twisted bilayer graphene: An analytical approach. *Phys. Rev. Research*, 2:023237, May 2020.

[7] Shang Liu, Eslam Khalaf, Jong Yeon Lee, and Ashvin Vishwanath. Nematic topological semimetal and insulator in magic angle bilayer graphene at charge neutrality. *arXiv preprint arXiv:1905.07409*, 2019.

[8] Nguyen N. T. Nam and Mikito Koshino. Lattice relaxation and energy band modulation in twisted bilayer graphene. *Phys. Rev. B*, 96:075311, Aug 2017.

[9] Cécile Repellin, Zhihuan Dong, Ya-Hui Zhang, and T. Senthil. Ferromagnetism in narrow bands of moiré superlattices. *Phys. Rev. Lett.*, 124:187601, May 2020.

[10] Zhida Song, Zhijun Wang, Wujun Shi, Gang Li, Chen Fang, and B. Andrei Bernevig. All magic angles in twisted bilayer graphene are topological. *Phys. Rev. Lett.*, 123:036401, Jul 2019.

[11] Grigory Tarnopolsky, Alex Jura Kruchkov, and Ashvin Vishwanath. Origin of magic angles in twisted bilayer graphene. *Phys. Rev. Lett.*, 122:106405, Mar 2019.

[12] Dillon Wong, Kevin P. Nuckolls, Myungchul Oh, Biao Lian, Yonglong Xie, Sangjun Jeon, Kenji Watanabe, Takashi Taniguchi, B. Andrei Bernevig, and Ali Yazdani. Cascade of transitions between the correlated electronic states of magic-angle twisted bilayer graphene. *arXiv e-prints*, page arXiv:1912.06145, December 2019.

[13] Ming Xie and A. H. MacDonald. Nature of the correlated insulator states in twisted bilayer graphene. *Phys. Rev. Lett.*, 124:097601, Mar 2020.

[14] Uri Zondiner, Asaf Rozen, Daniel Rodan-Legrain, Yuan Cao, Raquel Queiroz, Takashi Taniguchi, Kenji Watanabe, Yuval Oreg, Felix von Oppen, Ady Stern, et al. Cascade of phase transitions and dirac revivals in magic angle graphene. *arXiv preprint arXiv:1912.06150*, 2019.